Magnetic and structural investigation of the composition dependence of the local order in amorphous Tb-Fe

F. Hellman,* R. B. van Dover, S. Nakahara, and E. M. Gyorgy

AT&T Bell Laboratories, Murray Hill, New Jersey 07974

(Received 15 September 1988; revised manuscript received 31 October 1988)

The properties of ferrimagnetic amorphous Tb-Fe prepared by magnetron cosputtering over a range of composition from 9 to 40 at. % Tb have been extensively examined. No sign of crystallinity is found for any of these samples by transmission electron microscopy or x-ray diffraction. The gross properties such as saturation moment and Curie temperature are well behaved over this entire range. However, the magnetic anisotropy, which is an extremely sensitive probe of local structure, exhibits a relatively abrupt transition at 22 at. % Tb, the magnetic compensation composition. No change in such properties as anisotropy is expected to occur at the magnetic compensation composition, and indeed results to be described below suggest that this coincidence is simply accidental. Deposition parameters are varied in an attempt to understand the unexpected transition in the local structural order.

INTRODUCTION

Thin films of amorphous Tb-Fe (a-Tb-Fe) and related amorphous rare-earth–transition-metal (a-RE-TM) alloys are the leading candidates for magneto-optic recording, a high-bit-density, read-write storage technology.[1-3] In addition, from a purely scientific standpoint, these materials may be hoped to shed light on the structure of the amorphous phase as prepared by vapor deposition because they possess good metallurgic stability and, for most deposition procedures, a strong intrinsic uniaxial magnetic anisotropy perpendicular to the film plane, indicating some sort of as-yet not understood structural anisotropy built in by the growth process.[4,5] A complete set of measurements on well-characterized samples is thus of both technological and scientific interest.

Several different sources for the perpendicular anisotropy have been postulated for differently prepared films. Microscopic sources include so-called "pair ordering" due either to the preferential bonding of, for example, Tb atoms to Fe atoms during layer-by-layer growth[6-8] or to preferential resputtering of, for example, Gd from Gd-Co during growth by diode sputtering with a bias applied to the substrate.[5,9-11] This chemical ordering may more appropriately be termed chemical short-range order.[12] A second related microscopic possibility is that the local clusters of atoms characteristic of the amorphous phase[13-15] are oriented, also due to the growth process.[5] A third microscopic source, called bond-orientational anisotropy, depends neither on chemical ordering nor on the presence of local clusters, but on a difference in the number of neighbors in plane and out of plane due to relaxed growth-induced local stresses.[16] The next, more macroscopic, possible source of the anisotropy is a stress field perpendicular to the film acting in combination with the large magnetostriction that a-RE-TM films are believed to possess.[17-19] Stress may be present in the films due to differential thermal contraction of substrate and film or compaction of the film or Ar inclusion due to en-

ergetic particle bombardment during growth. Finally, amorphous films often possess a columnar microstructure due to limited surface mobility during growth;[20,21] oriented voids may also occur due to Ar bombardment and inclusion, particularly in diode-sputtered films prepared with a substrate bias.[22] A columnar microstructure can lead to a magnetic anisotropy due to preferential oxidation or segregation along the column faces.[22-24] Shape anisotropy is *not* expected to contribute significantly to the anisotropy induced by these columns unless the voids between the columns become approximately equal in volume to the columns.[25] Mizoguchi and Cargill present an overview of these possibilities and an analysis of how these structural anisotropies produce magnetic anisotropy.[26]

While all these sources almost certainly contribute in varying degrees to the anisotropy in any given film, it is possible in some cases to show that microscopic sources dominate. Direct evidence for pair ordering has been looked for by x-ray and electron diffraction in films prepared by various groups.[26-28] The results are so far inconclusive. Structural anisotropy has been measured by x-ray and neutron diffraction in *other* types (not a-RE-TM alloys) of bulk metallic glasses grown or annealed under stress.[29-31] Note that the anisotropy in the pair distribution functions necessary to explain the magnetic anisotropy of the a-RE-TM alloys is quite small.[9,26]

Previous studies of a-Tb-Fe films prepared by magnetron cosputtering have shown that the magnetic moment M and Curie temperature T_C are quite comparable to those of films prepared by other deposition methods such as diode sputtering or evaporation.[8,32] The microstructure of an amorphous film[32] and the magnitude of the intrinsic perpendicular uniaxial anisotropy K_{ui} depend somewhat more on the deposition method. As will be further discussed below, films prepared by magnetron cosputtering possess a large K_{ui}(6×10^6 ergs/cm^3 for samples deposited and measured at room temperature). The films are dense with no visible evidence of columns

or voids when examined by transmission electron micros-copy (TEM). Furthermore, the magnitude of K_{ui} has been found to increase significantly with increasing *deposition* temperature. This effect was described in Ref. 8 where it was shown that magnetron cosputtered samples grown at 77 K have a significantly reduced K_{ui} compared to those grown at room temperature. It has subsequently been found that samples grown at 180 °C possess a still greater K_{ui}. These results are also consistent with those reported by Takeno *et al.*[33] on flash-evaporated *a*-$Tb_{31}Fe_{69}$ and Kobayashi *et al.*[7] on electron-beam-deposited *a*-Tb-Fe. As observed in Ref. 8, the dependence of K_{ui} on the deposition temperature together with the known positive sign of the magnetostriction rule out stress induced by differential thermal contraction as the primary source of the intrinsic anisotropy. The dependence strongly suggests that the anisotropy in these magnetron-sputtered films is due to a model such as pair or cluster ordering which requires that a local equilibrium be achieved or at least approached. Increasing the deposition temperature increases the surface mobility, allowing the atoms to find more energetically favored locations, which in turn should increase the fraction of oriented pairs or clusters, thereby increasing K_{ui}. Note that by contrast, *a*-Gd-Fe does not apparently show K_{ui} increasing with deposition temperature, implying a different source of the anisotropy.[7]

It has previously been shown that the direction along which the uniaxial anisotropy lies in our films is not, in fact, strictly perpendicular, but lies at a small angle to the perpendicular.[34] This effect was uncovered in investigating the source of a *unidirectional* anisotropy induced in a crystalline Ni-Fe film grown in a bilayer with an amorphous Tb-Fe film. The induced preferred direction is directly related to the small in-plane component of the uniaxial anisotropy of the Tb-Fe. The angle of the uniaxial anisotropy is believed to be related to the incident angles of the Tb and Fe atomic beams during deposition.

Further investigation has shown the angle of the easy axis to be a complicated function of composition. In particular, a large discontinuity in the magnitude of the angle is found at 22 at. % Tb. In addition, we have made detailed measurements of the torque exerted on the sample by a magnetic field applied at various fixed angles to the sample. These measurements also reveal an abrupt change in behavior at 22 at. % Tb. The discontinuity is studied by varying such deposition parameters as the incident angles of the Tb and Fe atoms, the film thickness, and the substrate temperature, as well as by varying the temperature at which the uniaxial anisotropy is measured. No sign of this abrupt change is seen in the magnetic moment, Curie temperature, or resistivity. The magnetic anisotropy is, however, a far more sensitive probe of the local structure, as it depends on the locations of the neighbors, not just their numbers and distances.

We will show that the magnetic anisotropy of Tb-rich films can be described by a simple uniaxial form. By contrast, the magnetic anisotropy of Fe-rich films (those containing less than 22 at. % Tb) grown at room temperature requires a complex form which strongly suggests the presence of a second phase. The formation of this second phase depends on the deposition temperature; it does not form in Fe-rich samples grown at 77 K, as evidenced by the simple uniaxial anisotropy seen in these samples. Possible origins for the second phase are discussed in the section entitled "Model." Basic structural characterization and magnetic properties as a function of film composition, deposition parameters, and measurement temperature are presented.

EXPERIMENTAL PROCEDURE AND RESULTS

Samples are prepared in the dc magnetron system indicated schematically in Fig. 1. The Tb and Fe targets are arranged in a line parallel to the row of fused quartz substrates above. This line is defined in Fig. 1 to be the x axis. The geometry results in a composition spread across the row. Rates are monitored by an Inficon quartz-crystal monitor mounted next to the row of substrates. Since the Tb and Fe rates may be independently varied, any given composition may be obtained at any point along the row, thus allowing the incident angles of the Tb and Fe atoms to be varied independently of the composition. Substrate temperature is varied between 77 K and 800 °C in this work; depositions are primarily made onto substrates held nominally at room temperature. Unless explicitly otherwise stated, the reader should assume that the deposition was made at room temperature. Substrates may also be rotated during deposition, thereby greatly reducing any effect of the incident angles. Argon at a pressure of 5×10^{-3} Torr is the sputtering gas. Typical throttled background pressure prior to introducing the argon is 2×10^{-7} Torr, a pressure which is certainly further reduced by the gettering effect of the Tb atoms sputtered into the LN_2-cooled shroud surrounding the guns prior to deposition onto the substrates. Sample compositions are determined by Rutherford backscattering in conjunction with the deposition rates measured by a quartz-crystal rate monitor.

Tb-Fe films thus prepared are visually shiny. Ar and oxygen inclusion was measured by Auger depth profiling
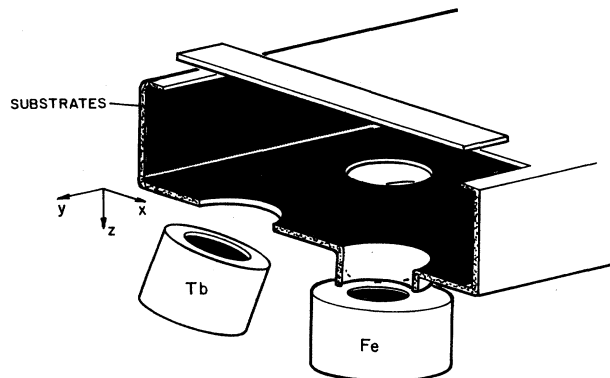

FIG. 1. Schematic of the sputtering system showing Tb and Fe magnetron guns, the row of substrates above, and the LN_2-cooled shroud. The x,y,z coordinate system is indicated on the left.

and was found to be below the detectable limit, i.e., considerably less than 1 at. %. Films examined by both bright- and dark-field TEM prove to be dense, featureless films at all compositions from 13 to 40 at. % Tb. The samples for TEM were 500 Å thick and were prepared by deposition directly onto C-coated Cu TEM grids. They were transferred from the sputtering system to the 120-keV Phillips 400 TEM quickly to limit the oxidation. Figure 2 shows the bright-field and selected-area-diffraction (SAD) images of a film containing 24 at. % Tb. Figure 3 shows the bright-field and SAD images of a film containing 17 at. % Tb. The bright-field images show a dense film with no obvious microstructure, such as columns or voids. The SAD pictures show halos characteristic of amorphous films. Dark-field images also show no structure. TEM shows that films deposited at room temperature containing 12 at. % Tb or less are partially crystallized.

X-ray diffraction measured in a diffractometer shows no sign of crystallinity for samples grown at room temperature with Tb concentrations as low as 9 at. % Tb. Samples containing less than 9 at. % Tb are partially crystallized; a sharp peak corresponding to α-Fe appears in addition to the amorphous background. Note that TEM revealed that 12-at. %-Tb samples are actually partially crystallized, despite appearing amorphous in (less-sensitive) x-ray-diffraction measurements. Samples grown at 200 and 400 °C are amorphous according to x-ray diffraction at 11.5 at. % Tb. At 600 °C the transition from crystallinity to the amorphous state occurs at approximately 19 at. % Tb. At 800 °C samples up to at least 35 at. % show strong crystalline peaks. Figure 4 summarizes the amorphous-crystalline phase diagram for as-grown samples based on x-ray diffraction. Note that this diagram does *not* reflect the crystallization temperature of films grown in the amorphous state; it shows instead the state of thin films grown on substrates held at various temperatures.

Figure 5 shows a comparison of the x-ray-diffractometer scans for a Tb-rich film containing 33 at. % Tb and an Fe-rich film containing 18.5 at. % Tb. These samples were deposited onto Si substrates. X-ray-diffraction patterns for samples deposited onto the usual fused-quartz substrates appear the same except for the additional structure due to the amorphous substrate which somewhat obscures the data. The average radial spacing d in the amorphous alloy is plotted in Fig. 6 and is approximately proportional to the Tb concentration. This spacing is based on the location of the 2θ peak maximum and takes into account the fact that x-ray scattering only measures the component of the radial spacing in the plane perpendicular to the scattering vector. A factor of 1.23 is necessary to convert this average in-plane component into an average radial spacing; thus $d = 1.23\lambda / 2\sin\theta_{max}$.[35] d ranges from 2.6 Å for a 14-at. %-Tb sample to 3.1 Å for a 40-at. %-Tb sample.

Figure 7 shows the magnetic moment M normalized to its room-temperature value as a function of temperature for five samples grown at room temperature. The Curie temperatures of these samples are consistent with those previously reported for a-Tb-Fe films.[4,8,36,37] These five curves show no unexpected anomalies; the compensation temperature for the 20.5-at. %-Tb sample is somewhat below room temperature, that of the 22.5-at. %-Tb sample is somewhat above. Since each of these samples has an approximately 2.5-at. % composition spread in it, M never goes identically to zero. These films are protected from oxidation by a 500-Å nonmagnetic overlayer. The moment was measured by the Faraday-balance technique in a field of approximately 6 kOe. The sample was heated to 160–200 °C in a furnace with flowing He gas. Data taken on cooling the sample, or on subsequent reheating, show some irreversible changes have taken place in samples containing less than 23 at. % Fe, indicating that these Fe-rich samples are more susceptible to irreversible structural changes than are the Tb-rich samples.

Figure 8 shows the room-temperature saturation moment M as determined in a vibrating-sample magnetometer (VSM); the maximum field was 15 kOe. Figure 8 also shows values determined by measuring the torque exerted on the sample by an applied magnetic field, as will be discussed below. The compositions of the samples were determined by Rutherford backscattering; there is an approximately 1-at. % composition spread per sample. M
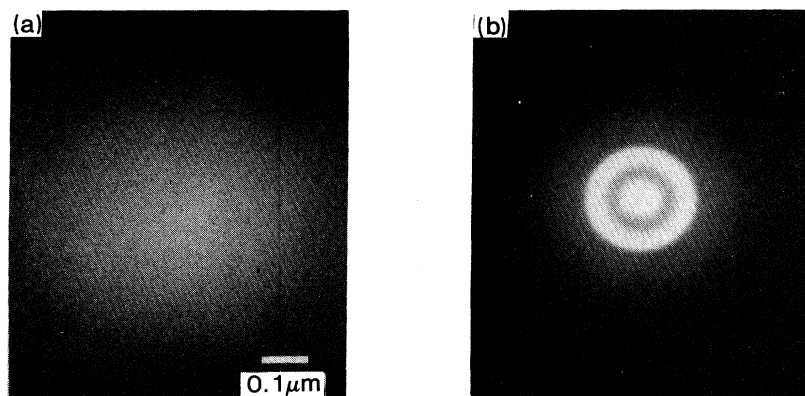

FIG. 2. TEM bright-field and selected-area diffraction images of a-Tb-Fe containing 24 at. % Tb.
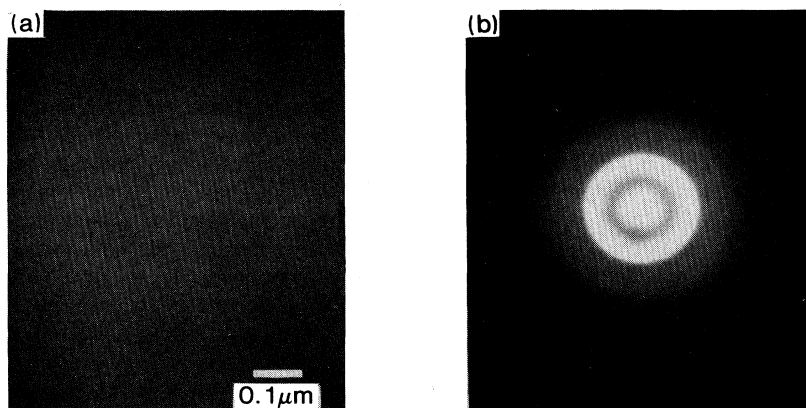
(a)   (b)

0.1 μm

FIG. 3. TEM bright-field and selected-area diffraction images of a-Tb-Fe containing 17 at. % Tb.

behaves reasonably for a ferrimagnetic material with a room-temperature compensation point near 21.5 at. % Tb.

Figure 9 shows the product of the room-temperature coercive force and magnetic moment $H_c M$ for the same samples. We chose to plot $H_c M$ rather than H_c since a more meaningful measure of the energy required to reverse the magnetization is achieved in this way. $H_c M$ is relatively constant through compensation, falling off at high and low Tb concentrations.

Thus in properties such as $M(T)$, H_c, x-ray diffraction, and TEM, these a-Tb-Fe films show no peculiar properties. However, when the magnetic anisotropy is measured in detail, striking peculiarities are found. Two types of characterization of the anisotropy were performed. First, the direction of the easy axis was examined. Second, the torque resulting from applying a magnetic field of varying strength at a fixed angle with respect to the easy axis was measured.

A recording torque magnetometer was used for both of these measurements. The principles of the torque magnetometer used for this experiment may be found, for exam-

ple, in Ref. 38. The torque on the sample is equal to $\mathbf{M} \times \mathbf{H}$, where $\mathbf{M} = M\hat{\tau}$ and $\hat{\tau}$ is a unit vector whose direction is determined by the magnitude and direction of the applied field $\mathbf{H}$ as well as by the anisotropy of the sample. The direction of the effective easy axis was measured by determining the angle of the field relative to the film surface when the torque equals zero. This condition requires that $\mathbf{H}$ be parallel to $\mathbf{M}$, which occurs when the field lies along an easy axis of the sample. The measurement procedure is to first determine on a fixed protractor the angle at which the applied magnetic field is parallel to the plane of the sample, using a laser and mirror system. Next, the magnetic field is turned on, and the magnet is rotated until the measured torque equals zero; the angle on the protractor is then noted. If the sample is to be measured at LN_2 temperatures, it is then cooled with the field applied along the easy axis. This procedure is necessary to prevent any domain structure from being "frozen in" due
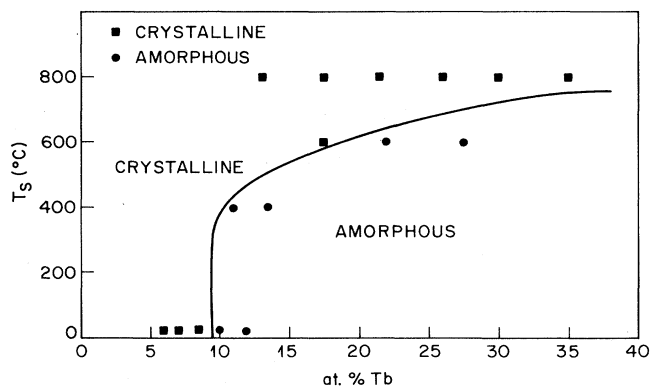
FIG. 4. Amorphous-crystalline phase diagram for as-grown samples based on x-ray diffraction. The y axis is the temperature of the substrates during deposition. Samples above and to the left of the line were determined to be crystalline; samples below and to the right were amorphous.
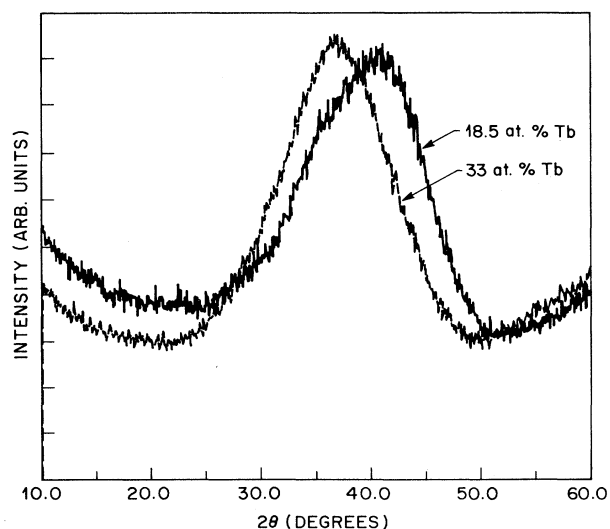
FIG. 5. X-ray-diffractometer scans for a-Tb-Fe containing 33 and 18.5 at. % Tb. Scattering angle is normal to the substrate. Samples are 5500 Å thick and were grown at room temperature on Si substrates.
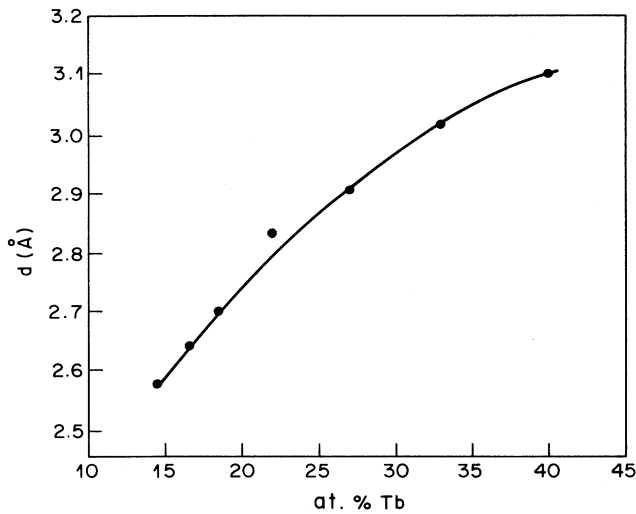
FIG. 6. Average radial spacing $d = 1.23\lambda/2\sin\theta_{max}$ as a function of composition. Samples are 5500 Å thick and were grown at room temperature on Si substrates.

to the extremely high coercive force of these materials at low temperatures. The easy axis at $T=77$ K is then determined by again measuring the angle at which zero torque occurs.

Figure 10 shows the compositional dependence of the direction of the easy axis projected into the x-z and y-z planes, measured from the perpendicular, for 5500-Å-thick samples deposited onto room-temperature substrates. The x axis lies along the line connecting the Tb
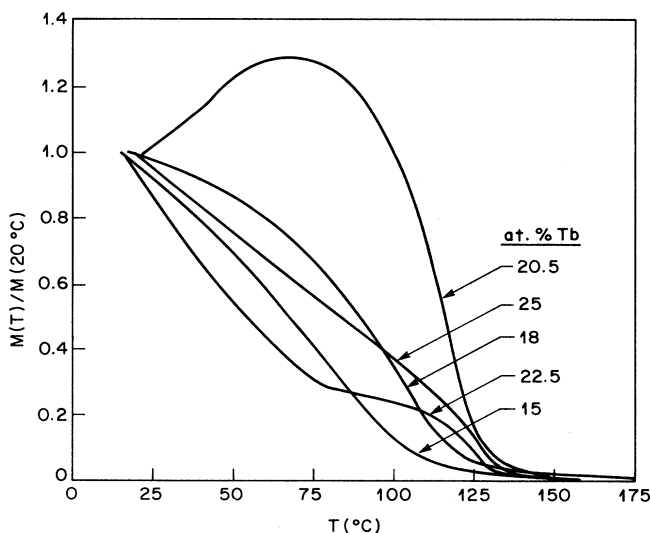

FIG. 7. Magnetic moment as a function of temperature normalized to the room-temperature moment. Data were measured by the Farraday-balance technique; the field at the samples was 6 kOe. Samples were heated at approximately 6°/min in a furnace with flowing He gas. Samples are 5500 Å thick and were grown at room temperature. They are protected from oxidation by a 250 Å Nb overlayer.
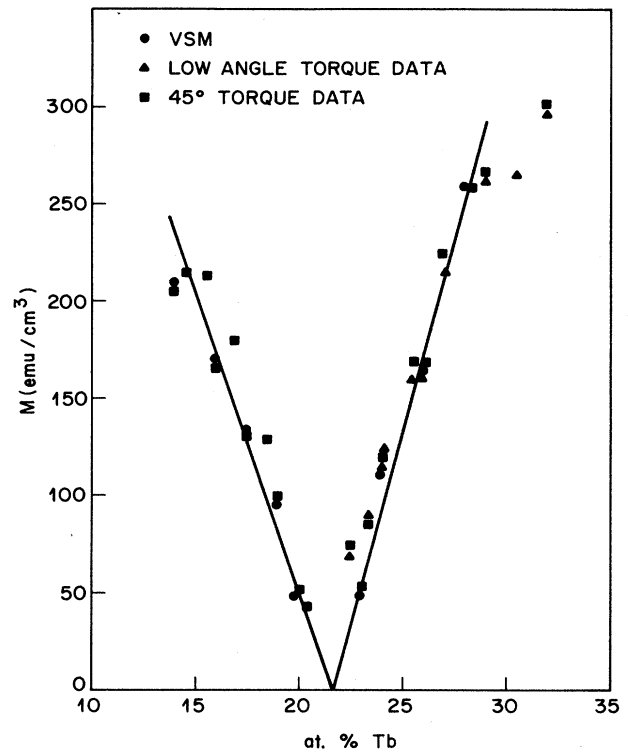

FIG. 8. Room-temperature moment M as a function of composition determined by vibrating-sample–magnetometer and torque measurements at fixed angles. Samples are 5500 Å thick and were grown at room temperature. The lines are drawn to guide the eye and are primarily fit to the VSM data.

and Fe sources as described above and shown schematically in the corner of Fig. 10. The y axis is the other in-plane direction. These samples were all from one deposition run; hence the incident angles of the Tb and Fe atoms vary along with the composition. The easy axis lies purely in the x-z plane; it is tilted towards the Fe source for all compositions above about 15 at. % Tb, crossing over to tilt towards the Tb source at the substrate position (parametrized by composition) at which
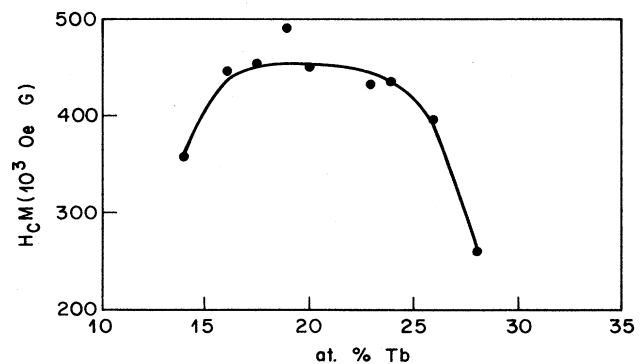

FIG. 9. Product of the room-temperature coercive force and magnetic moment H_cM as a function of composition. Samples are 5500 Å thick and were grown at room temperature.
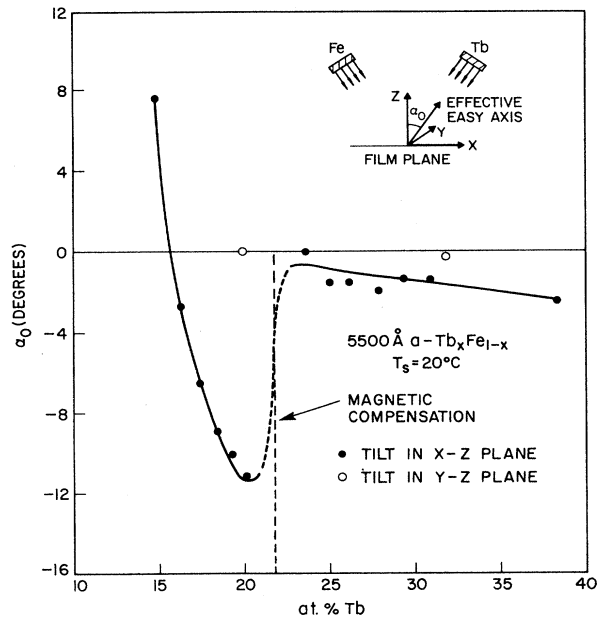
FIG. 10. Direction of the effective easy axis measured from the perpendicular as a function of composition in both the x-z and y-z planes. A simplified schematic is shown in the upper right-hand corner. The solid line is drawn to guide the eye; the dashed line indicates the region where samples are too close to the magnetic compensation composition to be measured. Samples are 5500 Å thick and were grown at room temperature.

the net incident angle (defined as the sum of the Tb and Fe incident angles weighted by their atomic percentage) is perpendicular. There is no tilt in the y-z plane. There is also no tilt for samples deposited onto a rotating substrate. These results support the conclusion drawn in Ref. 34 that the tilt is due to the incident angles of the atoms.

The compensation composition at 22 at. % Tb is indicated on the figure. Samples cannot be measured between 21 and 23 at. % Tb, as shown in the figure by the long-dashed line, both because the moment and hence the torque is too small and, more importantly, because the coercive force is too high to allow the samples to be magnetically saturated by the field we have available for this measurement (20 kOe). Above this composition range, the tilt is small and varies slowly with composition. Below this region, the tilt is initially quite large and varies strongly with composition.

Figure 11 shows the deviation from perpendicular as a function of composition for samples from different runs with different Tb and Fe incident angles. The Tb and Fe incident angles are necessarily related to each other and, as mentioned above, vary along with the composition. Each set of data has been characterized in the figure by the angles at the substrate position where 22 at. % Tb occurs. The tilt for samples containing more than 22 at. % Tb is not a strong function of incident angle. By contrast, both the size of the apparent discontinuity at 22 at. % Tb and the subsequent composition dependence on the Fe-rich side of 22 at. % Tb is strongly dependent on
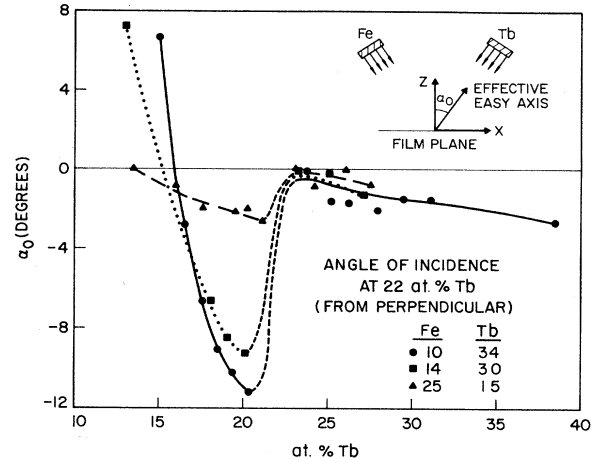

FIG. 11. Direction of the effective easy axis measured from the perpendicular as a function of composition for three different runs with different angles of the incident atoms. The lines are drawn to guide the eye; the dashed line in each of the three indicates the region where samples cannot be measured. The solid curve with the solid circles represents the same data presented in Fig. 10. Samples are 5500 Å thick and were grown at room temperature.

incident angle. Note particularly that the discontinuity remains fixed at the magnetic compensation composition (22 at. % Tb).

Figure 12 shows the deviation from perpendicular for Tb-Fe samples of two different thicknesses: 5500 and 700 Å. Both sets of samples were grown with the set of incident angles of Fig. 10, i.e., Fe at 10° and Tb at 34° for the 22-at. %-Tb samples of each thickness. On the Tb-rich side the angle is independent of thickness, while on the Fe-rich side it is strongly dependent.
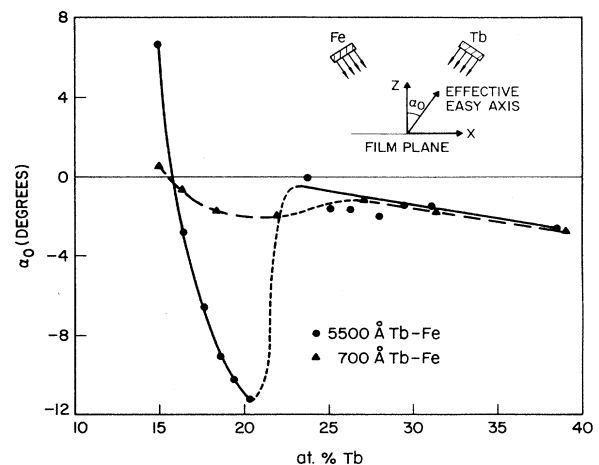

FIG. 12. Direction of the easy axis measured from the perpendicular as a function of composition for two film thicknesses. The solid circles are again the data shown in Fig. 10. The thin samples, represented by open circles, were prepared with the same incident angles as the thick samples, represented by the solid circles. Samples were grown at room temperature.

The magnitude of the intrinsic anisotropy is a strong function of measurement temperature, most likely due to an increase in the single-ion anisotropy accompanying the increase in the subnetwork moments with decreasing thermal disorder.[39] The coercive force at 77 K in nearly all the a-Tb-Fe samples is greater than 20 kOe, the field available to us for measurement. As discussed previously, samples are therefore magnetized along an easy-axis direction at room temperature and cooled with the field on along this axis. The easy axis at 77 K is in no sample more than 25° away from the axis at room temperature; the sample therefore presumably remains in a single-magnetic-domain configuration on cooling. The dashed region, representing samples whose easy-axis angle could not be measured, is wider in Fig. 13 than in Figs. 10 and 11. This widening is because the direction of the magnetic moments of the Tb and Fe subnetworks for samples whose composition lies between the compensation composition at room temperature and at 77 K must reverse. However, the enormous increase in coercive force prevents this reversal. The magnetization of these samples is thus frozen into some unknown domain configuration in which M is not necessarily parallel to the field; hence the easy axis at 77 K cannot be determined. Figure 13 only shows data for samples measured first at room temperature, then cooled and successfully measured at 77 K, and so has fewer data points than Figs. 10 and 11.

Figures 13(a) and 13(b) show the results of measuring the tilt at LN_2 temperature for two different sets of incident angles. Note both the similarities between the composition dependences shown in Figs. 13(a) and 13(b) and the different y-axis scales. The data shown by solid circles in each are taken at room temperature. Figure 13(a) shows data for the same samples as were used for Fig. 10; Fig. 13(b) shows data for the samples used for the shallowest curve in Fig. 11. The discontinuity at 22 at. % Tb is quite striking: more than 30° in Fig. 13(a) and 8° in Fig. 13(b). On the Tb-rich side, the tilt is relatively independent of measurement temperature. On the Fe-rich side, by contrast, there is a strong dependence on measurement temperature.

The fact that the discontinuity occurs at the magnetic compensation composition is peculiar. In order to test whether this effect is truly magnetic in origin, or is simply due to an unlikely but nonetheless possible coincidence, samples were deposited onto substrates held at 180 °C, substantially above the Curie temperature for all compositions studied. Figure 14 shows the resulting direction of the easy axis measured at room temperature. These samples were prepared with the incident angles of the samples of Fig. 10, which showed the largest discontinuity. The magnitude of the tilt on the Fe-rich side is greatly reduced, but the discontinuity is still clearly visible at the magnetic compensation composition. It is not possible to entirely rule out by this experiment any effects of the magnetic compensation, since the sample is, of course, measured below the Curie temperature, but it supports the conclusion that the coincidence of the discontinuity with compensation truly is coincidental. Further experiments with other a-RE-Fe alloys might

better test this conclusion, as compensation occurs at different compositions.

Samples were also deposited onto substrates held at 77 K, again with the incident angles of the samples of Fig. 10. The magnitude of the intrinsic anisotropy at room temperature is reduced in samples grown at 77 K compared to those grown at room temperature. This reduction in the perpendicular intrinsic anisotropy causes the shape anisotropy to dominate at lower values of M, causing the effective easy axis to fall into the plane at compo-
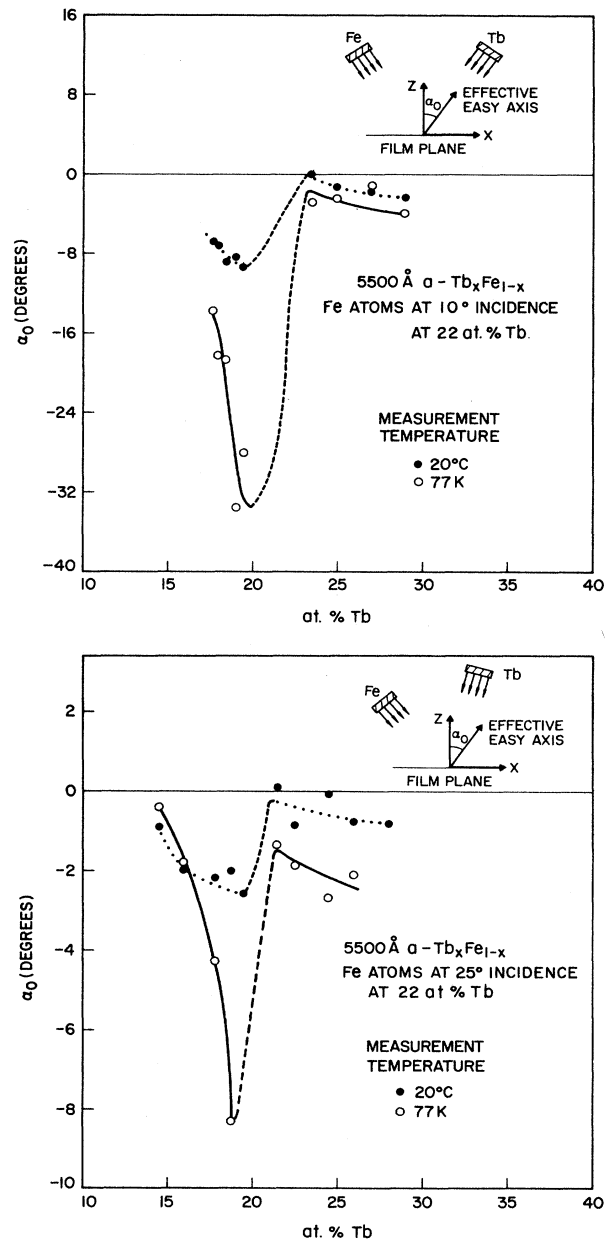

FIG. 13. Direction of the easy axis measured at room temperature (solid circles) and at LN_2 temperature (open circles). (a) Samples with the lowest Fe incident angle at 22 at. % Tb, as shown in Figs. 10 and 11. (b) Samples with the highest Fe incident angle at 22 at. % Tb, as shown in Fig. 11.
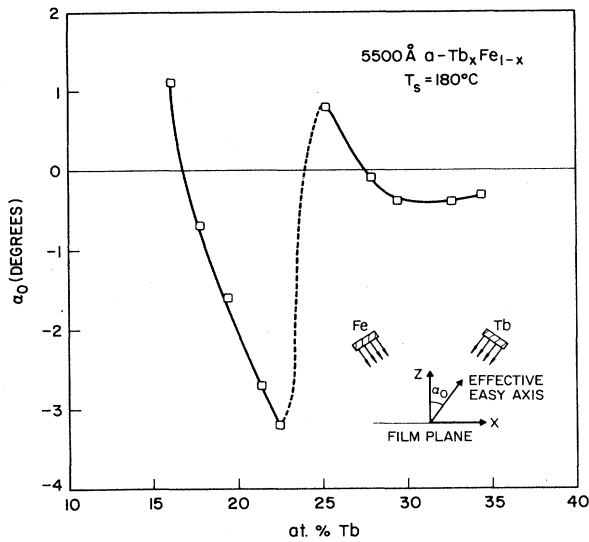
FIG. 14. Direction of the easy axis measured at room temperature for samples grown at 180 °C, above the Curie temperature.

sitions close to 22 at. % Tb. The results are shown in Fig. 15. The tilt for all compositions is *greatly* increased, presumably because the reduced surface mobility during growth increases the effect of the nonperpendicular incident angles of the atoms. There is, however, no discontinuity seen. This fact implies that the source of the discontinuity, presumably an abrupt change in the local order, does not occur in samples grown at 77 K.

We turn now to torque measurements as a function of field with the field held at a fixed angle α. It will be shown in the next section that when $|\alpha| \ll 1$ rad or $=45°$ away from the effective easy axis α_0, the torque data may be relatively easily interpreted for samples with simple uniaxial anisotropy. We will consider a sample in an applied field H at an angle α to the perpendicular. The sample has magnetic moment M, uniaxial anisotropy con-
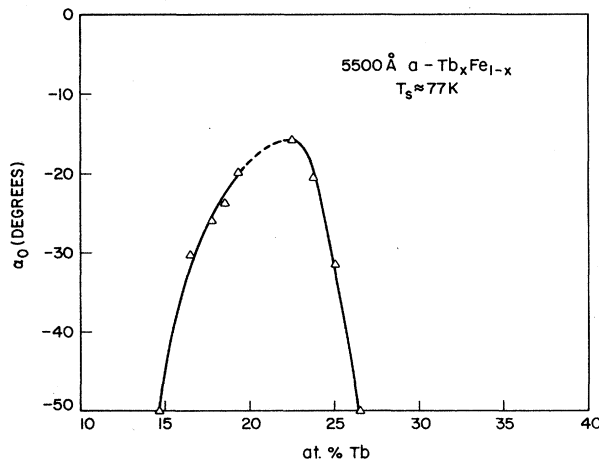
stant K_{ui}, an intrinsic easy axis at an angle β to the perpendicular, and an effective easy axis at an angle α_0. The relationship between β and α_0 will be discussed in the next section. An equation for $(L/H)^2$ may be derived for $\alpha = \alpha_0 \pm 45°$:

$$\left[\frac{L}{H}\right]^2 = \frac{-M^2}{2K}L + \frac{1}{2}M^2 , \tag{1}$$

where L is the torque per unit volume of the sample and

$$K \equiv K_{ui}\cos2(\alpha_0 - \beta) - 2\pi M^2\cos2\alpha_0 .$$

This equation was originally derived by Miyajima *et al.* for $\alpha_0 = \beta = 0$.[40] The function $(L/H)^2$ is linear in L and has a slope and intercept which lead directly to K_{ui} and M. In the other limit, $\alpha = \alpha_0 \pm \epsilon$, where ϵ is a small angle, an equation for $H\epsilon/L$ may be derived:

$$\frac{H}{L}\epsilon = \frac{H}{2K} + \frac{1}{M} , \tag{2}$$

where K is again defined as above. This expression is linear in H. This equation was briefly discussed by Chikazumi, again for $\alpha_0 = \beta = 0$.[41] The intercept and slope lead directly to values for K_{ui} and M.

The torque–versus–applied-field data is taken by finding the easy axis as described above, ramping the field up to 24 kOe, well above H_c at room temperature for any of the samples measured, then rotating the magnet to the appropriate angle and measuring the torque as the field is decreased. Data will be presented for samples similar to those showing the most dramatic discontinuity in the angle, plotted in Fig. 10. Figures 16(a) and 16(b) show plots for $\alpha = \alpha_0 \pm \epsilon$ and $\alpha_0 \pm 45°$, respectively, for a typical Tb-rich sample. These plots are well behaved; values for K_{ui} and M are easily found. Values for M from both sets of data are plotted in Fig. 8 along with the VSM data. Figures 17(a) and 17(b) show the same plots for a typical Fe-rich sample. The low-angle data are clearly nonlinear both in H and in ϵ; no meaningful values for M or K_{ui} could be determined. The 45° data are better behaved, but still show an asymmetry between $\pm45°$. Values for M were obtained by averaging the $\pm45°$ data; this procedure yielded numbers very close to those obtained from VSM data. These are plotted in Fig. 8. All Tb-rich samples behave as in Fig. 16. All Fe-rich samples grown at room temperature behave as in Fig. 17, with particular details of the plots varying. Values for the magnitude of the anisotropy versus composition are plotted in Fig. 18. This figure, the data, and the interpretation will be extensively discussed below when Eqs. (1) and (2) are derived.

Torque data (taken at room temperature) on Fe-rich samples grown at 77 K do not show the nonlinearities and asymmetries seen in Fig. 17. The data appear as in Fig. 16 and may be easily interpreted in terms of a uniaxial anisotropy. This lack of anomalous behavior is consistent with the continuity in α_0 through 22 at. % Tb seen in Fig. 15 and discussed briefly above. The transition in the local order reflected in the transition in the magnetic anisotropy of samples grown at room temperature is thus *not* seen in samples grown at 77 K.

FIG. 15. Direction of the easy axis measured at room temperature for samples grown at 77 K.

DISCUSSION AND DATA ANALYSIS

Figures 10–17 show a striking difference in the properties of room-temperature-deposited a-Tb-Fe containing less than 22 at. % Tb compared with that containing more. On the Tb-rich side, the angle of the effective easy axis α_0 is small, independent of deposition variables and relatively independent of measurement T. The torque plots are well behaved and independent of the sign of the angle of **H** with respect to the easy axis. On the Fe-rich side, α_0 is large, and strongly dependent on deposition variables and on measurement T. The torque plots cannot be interpreted in terms of the expressions in Eqs. (1) and (2); they depend strongly on the sign of the angle of **H** with respect to the easy axis. Samples grown at $180\,^{\circ}$C, above the Curie temperature, still show this transition occurring at 22 at. % Tb. The transition, however, goes away for samples deposited at 77 K, for which all torque data appear well behaved. The relatively abrupt transition does not appear to be reflected in TEM, in x-ray diffraction, or in properties such as the magnetic moment or the resistivity.

We will first consider how to write the magnetic energy of this material. We will derive Eqs. (1) and (2) and then consider what corrections are necessitated to the energy expression both by the nonlinearities seen in Figs. 16 and 17 and by the dependence on measurement temperature of α_0. The magnetic energy per unit volume of a thin-film sample with uniaxial anisotropy constant K_{ui} and magnetic moment M whose intrinsic easy axis is at angle β to the normal may be written

$$E = -\mathbf{H}\cdot\mathbf{M} + K_{ui}\sin^2(\theta-\beta) - 2\pi M^2\sin^2\theta , \tag{3}$$

where θ is the angle between $\mathbf{M}$ and the normal to the film. The derivative of E with respect to θ, $dE/d\theta$, must equal zero. Therefore,

$$\frac{dE}{d\theta} = -MH\sin(\alpha-\theta) + K_{ui}\sin2(\theta-\beta)$$

$$-2\pi M^2\sin2\theta$$

$$= 0 , \tag{4}$$

where α is the angle between $\mathbf{H}$ and the normal. The torque per unit volume of sample $L = \mathbf{M}\times\mathbf{H} = MH\sin(\alpha-\theta)$. At the easy axis, $L=0$ and $\alpha\equiv\alpha_0=\theta$. The true angle of the anisotropy, β, is then related to α_0, the measured angle where the torque equals zero, by the following expression:

$$K_{ui}\sin2(\alpha_0-\beta) = 2\pi M^2\sin2\alpha_0 . \tag{5}$$

The result of this correction is that $\beta\approx\alpha_0$ for samples closest to compensation where M is very small, and that
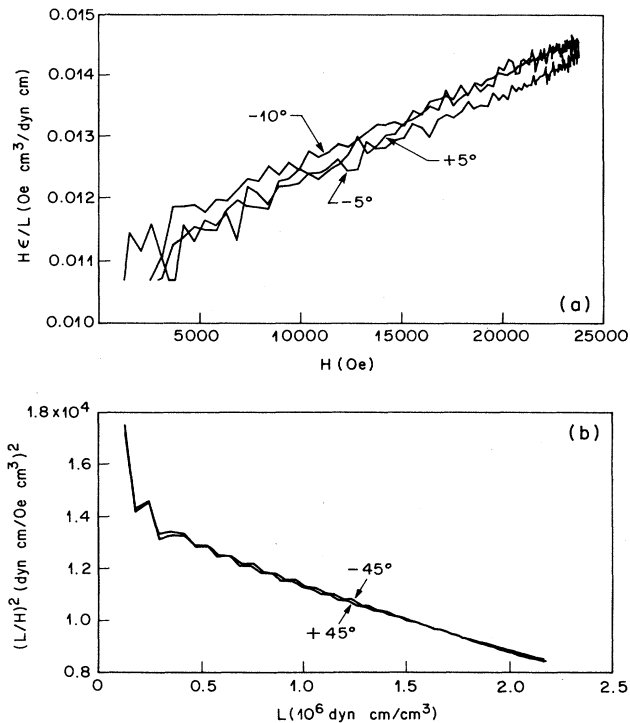

FIG. 16. Torque per unit volume at fixed angle for Tb-rich a-Tb-Fe. (a) Low-angle data: $\pm5^{\circ}$ and -10° for a 23.5-at. %-Tb sample. (b) $\pm45^{\circ}$ data for a 25.5-at. %-Tb sample. Angles are measured relative to the effective easy axis α_0. Samples are 5500 Å thick and were grown at room temperature.

FIG. 17. Torque per unit volume at fixed angle for Fe-rich a-Tb-Fe. (a) Low-angle data: $\pm5^{\circ}$ and $\pm10^{\circ}$ for a 19.5-at. %-Tb sample. (b) $\pm45^{\circ}$ data for an 18.5-at. %-Tb sample. Angles are measured relative to the effective easy axis α_0. Samples are 5500 Å thick and were grown at room temperature.
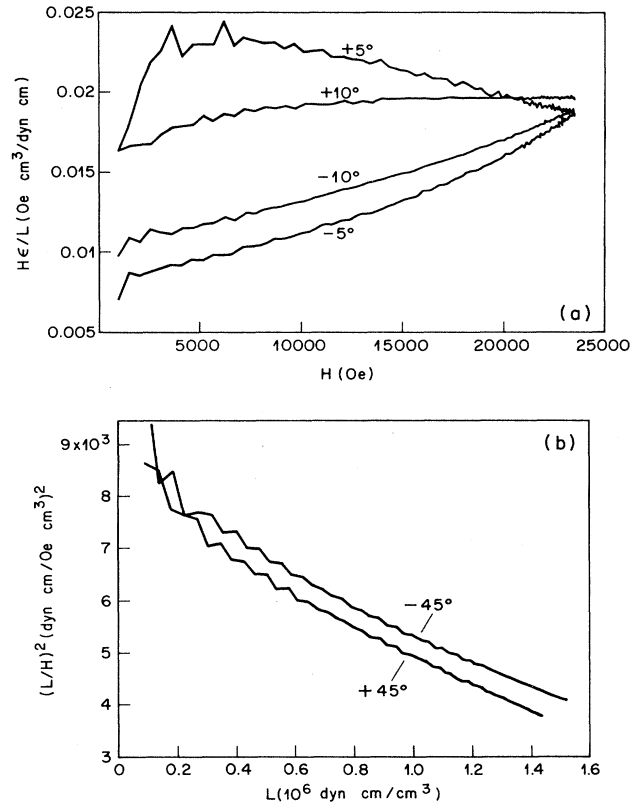
β is increasingly closer to the perpendicular axis than the measured angle α_0 the further from compensation the sample lies. Thus Figs. 10 and 11 should be corrected as follows: On the Tb-rich side of 22 at. % Tb the already small composition dependence of the tilt is reduced further, but on the Fe-rich side below 20 at. % Tb the already steep dependence will be increased.

Choosing $\alpha = \alpha_0 + 45°$, we may write

$$\sin 2\theta = -\sin 2(\alpha - \theta - \alpha)$$

$$= \sin 2(\alpha - \theta)\sin 2\alpha_0 + \cos 2(\alpha - \theta)\cos 2\alpha_0$$

and

$$\sin 2(\theta - \beta) = -\sin 2(\alpha - \theta + \beta - \alpha)$$

$$= \sin 2(\alpha - \theta)\sin 2(\alpha_0 - \beta)$$

$$+ \cos 2(\alpha - \theta)\cos 2(\alpha_0 - \beta) .$$

Substituting these expressions into Eq. (4), and using Eq. (5) to cancel terms containing

$$K_{ui}\sin 2(\alpha_0 - \beta) - 2\pi M^2 \sin 2\alpha_0 ,$$

we obtain

$$0 = -L + [K_{ui}\cos 2(\alpha_0 - \beta)$$

$$- 2\pi M^2 \cos 2\alpha_0]\cos 2(\alpha - \theta) .$$

Writing

$$\cos 2(\alpha - \theta) = 1 - 2\sin^2(\alpha - \theta) = 1 - 2(L/MH)^2$$

and rearranging terms, we obtain Eq. (1).

Choosing $\alpha = \alpha_0 + \epsilon$, where $\epsilon \ll 1$ rad, we write

$$\sin 2\theta = -\sin 2(\alpha - \theta)(\cos 2\alpha_0 - 2\epsilon \sin 2\alpha_0)$$

$$+ \cos 2(\alpha - \theta)(\sin 2\alpha_0 + 2\epsilon \cos 2\alpha_0)$$

and

$$\sin 2(\theta - \beta) = -\sin 2(\alpha - \theta)$$

$$\times [\cos 2(\alpha_0 - \beta) - 2\epsilon \sin 2(\alpha_0 - \beta)]$$

$$+ \cos 2(\alpha - \theta)$$

$$\times [\sin 2(\alpha_0 - \beta) + 2\epsilon \cos 2(\alpha_0 - \beta)] .$$

In the limit of small ϵ, M must also lie near the easy axis. Since $\alpha - \theta$ is small, $L/MH \ll 1$. Therefore,

$$\sin 2(\alpha - \theta) \approx 2\frac{L}{MH}$$

and

$$\cos 2(\alpha - \theta) \approx 1 .$$

Substituting these expressions into Eq. (4) and again cancelling terms using Eq. (5),

$$0 = -L - [K_{ui}\cos 2(\alpha_0 - \beta)$$

$$- 2\pi M^2 \cos 2\alpha_0](2L/MH - 2\epsilon) .$$
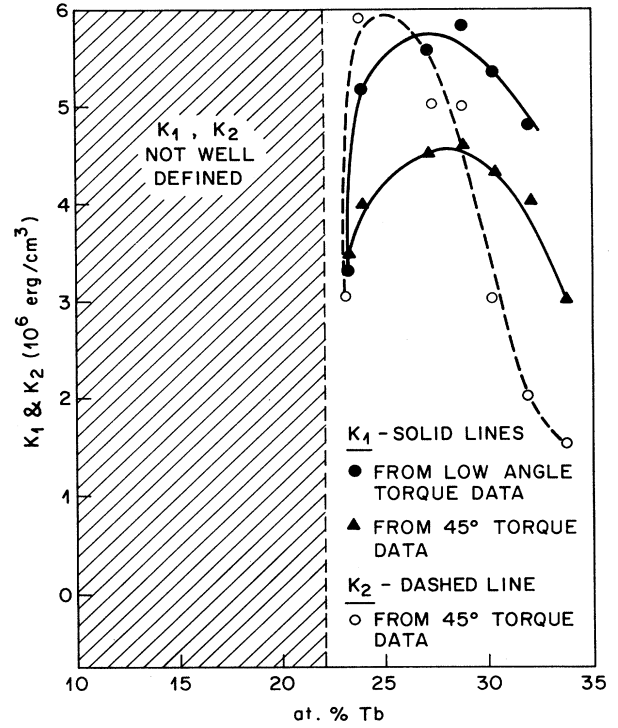
Rearranging we obtain Eq. (2).

FIG. 18. Room-temperature intrinsic uniaxial anisotropy constants K_1 (solid line) and K_2 (dashed line) as a function of composition determined by torque measurements at $\pm 45°$ (for both K_1 and K_2) and $\pm 5°$ and $\pm 10°$ (for K_1) with respect to the effective easy axis. Samples are 5500 Å thick and grown at room temperature. The lines are drawn to guide the eye. K_1 may be directly compared with values for K_{ui} in the literature.

The Tb-rich samples appear to be relatively well described by Eqs. (1)–(5), except for a curvature in $(L/H)^2$ at high L in the 45° plots for many of the samples. [It should be noted that the data in Fig. 16(b) show less curvature than most.] This curvature may be dealt with by adding the next term in the expansion of the anisotropy energy: $K_2\sin^4(\theta - \beta)$. The necessity of including the second-order term in the expansion of the anisotropy energy was also noted by Wolniansky et al.[42] Since α_0 for the Tb-rich samples measured is less than 3° and β is consequently even smaller, we will approximate the anisotropy energy as

$$E_{an} = K_1\sin^2\theta + K_2\sin^4\theta - 2\pi M^2\sin^2\theta \qquad (6)$$

and neglect β. Then

$$\frac{dE}{d\theta} = 0 = -MH\sin(\alpha - \theta) + K_1\sin 2\theta$$

$$- 2\pi M^2\sin 2\theta + K_2\sin 2\theta - \frac{K_2}{2}\sin 4\theta . \qquad (7)$$

The expression derived for the low-angle torque is identical to Eq. (2) (with α_0 and β set equal to zero) to order ϵ. The linearity in particular is unaltered. The expression for $(L/H)^2$ obtained for the 45° data becomes more complicated:

$$\left[\frac{L}{H}\right]^2 = -\frac{M^2 L}{2K} + \frac{M^2}{2}$$
$$+ \frac{K_2}{K}\left[1 - \left[\frac{L}{MH}\right]^2\right]^{1/2}$$
$$\times \left[-M\frac{L}{H} + \frac{2}{M}\left[\frac{L}{H}\right]^3\right], \qquad (8)$$

where K has been redefined:

$$K \equiv K_1 + K_2 - 2\pi M^2 .$$

$(L/H)^2$ is no longer linear in L.

We have fitted the 45° data for the Tb-rich samples to Eq. (8) and the low-angle data to Eq. (2) and have obtained values for K_1 and K_2. Figure 18 shows the values thus obtained. K_1 determined from Eq. (8) has approximately the same value as would be determined by a linear fit to the low torque, which is equivalent to the low-field portion of the curved 45° data. Mathematically, the initial slope of $(L/H)^2$ versus L may be determined by taking the total derivative d/dL of Eq. (8) and solving for $d/dL(L/H)^2$ at $(L/H)^2 = M^2/2$, its initial value:

$$\frac{d}{dL}\left[\frac{L}{H}\right]^2\Bigg|_{(L/H)^2 = M^2/2} = -\frac{M^2}{2(K_1 - 2\pi M^2)} .$$

Alternatively, we may take Eq. (7) in the limit of low fields; since the angle θ is then small, $\sin2\theta \approx 2\theta$ and $\sin4\theta \approx 4\theta$. Then, again substituting in for

$$2\theta \approx \sin2\theta = 1 - 2(L/MH)^2$$

as above, noting that the terms involving K_2 cancel,

$$0 = -L + (K_1 - 2\pi M^2)[1 - 2(L/MH)^2] .$$

Solving for $(L/H)^2$, we obtain Eq. (1), which was derived assuming $K_2 = 0$. Thus K_1 may be directly compared with the literature values for K_{ui} which are usually determined by a straight line fit to 45° data taken to lower fields than the 24 kOe in this work. The values for K_1 shown in Fig. 18 are very large compared even to other results for magnetron-sputtered samples. This fact is attributed to subtleties in the deposition parameters. Note that the large discrepancy seen in Fig. 18 in values for K_1 between the 45° and low-angle data, to be discussed below, make it obvious that when comparing values for the anisotropy, similar measurement techniques must be used. The values for K_2 are comparable to the value found for a-Tb$_{28}$Fe$_{72}$ by Wolniansky et al.[42] As discussed previously, K_1 can be made larger still by growing samples at higher deposition temperatures, necessarily below the crystallization temperatures shown in Fig. 4, however-er.

Figure 18 also shows two interesting facts. First, the value for K_1 derived from the low-angle data is higher than that derived from the 45° data. This discrepancy is an indication that the description of the anisotropy energy is still incomplete. In particular, it is likely to be necessary to include the fact that there is not a single easy axis, but a cone of them averaging to some effective

intrinsic easy axis. This latter description is more appropriate to an amorphous material and has been previously suggested for Gd-Co.[43] Rhyne et al. have measured neutron scattering, which suggests a cone of locally oriented moments M.[44]

The other interesting feature seen in Fig. 18 is the drop in K_1 below 27 at. % Tb. It appears from Fig. 18 that K_1 is headed for zero near the magnetic compensation point, an unexpected result. In a classic ferrimagnet, such as the garnets, K_{ui} is well behaved through the compensation point. The coercive force of these samples is still well below 24 kOe, and the data used to obtain K_1 appear well behaved; hence there is no obvious reason to discount these results. The most reasonable explanation is that K_1 is heading towards zero, due in some way to a phase transition at 22 at. % Tb or that a magnetostatic effect is, in fact, playing some role in K_1. It is important, however, to note that no drop is seen in $H_c M$ for the same samples near 22 at. % Tb (see Fig. 9). Generally, $H_c M$ would be expected to be related to K_{ui}. H_c is, however, at least a factor of 5 smaller than $H_K = 2K_{eff}/M$, the anisotropy field, and thus it is not energetically required that K_1 and $H_c M$ should show similar trends. Without a better understanding of the mechanism for magnetization reversal, it is difficult to know how H_c and K_{ui} should be related. Nonetheless, the lack of agreement between Figs. 9 and 18 is surprising. It should be noted that the significantly lower fields used for measurements of K_{ui} quoted in the literature do not permit K_{ui} to be determined for compositions close enough to compensation for the drop to be observed.

The interpretation of the data for the Fe-rich samples deposited at room temperature is far less straightforward. Consider the measurements of the Fe-rich material at LN_2 temperatures shown in Figs. 13(a) and 13(b). It is experimentally observed that the coercive force H_c and the anisotropy field $H_K = 2(K_{ui} - 2\pi M^2)/M$ are greatly increased at low temperatures. The saturation moment M is a weaker function of temperature: it depends only on the difference in the temperature dependencies of the two subnetworks. Looking at Eq. (5), for α_0 to increase with reduced temperature β, the direction of the intrinsic easy axis must be a function of temperature. Introducing the next order term at the *same* angle β as was done above for the Tb-rich material, i.e., $K_2\sin^4(\theta - \beta)$, causes Eq. (5) to be modified. The effective easy axis α_0 is then given by

$$(-K_{ui} - K_2)\sin2(\alpha_0 - \beta) + 2\pi M^2\sin2\alpha_0$$
$$+ \frac{K_2}{2}\sin4(\alpha_0 - \beta) = 0 .$$

We may expand $\sin2(\alpha_0 - \beta) \approx 2(\alpha_0 - \beta)$ and $\sin4(\alpha_0 - \beta) \approx 4(\alpha_0 - \beta)$ since both α_0 and β are empirically relatively small angles and necessarily of the same sign. The terms depending on K_2 then cancel and we are left with Eq. (5) again and the conclusion that, for α_0 to increase with K_{ui}, β must increase. Thus one possible expression for the anisotropy energy for the Fe-rich a-Tb-Fe which would explain Fig. 13 is $K'_{ui}\sin^2(\theta - \beta')$ where both K'_{ui} and β' are strong functions of temperature and are un-

equal to the K_{ui} and β which describe the Tb-rich material. Strain produced by differential thermal contraction of sample and substrate could produce a temperature-dependent β' by distorting the local arrangement of atoms. Alternatively, the faster increase of the Tb moment relative to the Fe moment with decreasing temperature could shift the angle. A change from 8° to 32° is large, but without further knowledge of the atomic arrangement producing the anisotropy, it is not possible to say whether or not this large change in α_0 can be accounted for by a temperature-dependent β.

A second possibility is that the anisotropy energy of the Fe-rich material deposited at room temperature must be written as

$$E_{an} = K_1 \sin^2(\theta - \beta) - 2\pi M^2 \sin^2\theta$$
$$+ K_2' \sin^4(\theta - \beta') , \qquad (9)$$

where now only K_1 and K_2' are assumed to be strong functions of temperature. Note the presence of two distinct angles, β and β', in Eq. (9), unlike the anisotropy energy of the Tb-rich material which could be described with a single small intrinsic angle, set equal to zero in obtaining Eq. (6). Equation (9) is more properly written as

$$E_{an} = K_i \sin^2(\theta - \beta_k) + K_j \sin^4(\theta - \beta_k)$$
$$+ K_i' \sin^2(\theta - \beta_k') + K_j' \sin^4(\theta - \beta_k') - 2\pi M^2 \sin^2\theta$$
$$(10)$$

allowing for lower- and higher-order terms at each intrinsic angle β_k and β_k'. The two quadratic and two quartic terms may be combined to give Eq. (9). The effective easy axis α_0 now may be written

$$-K_1 \sin 2(\alpha_0 - \beta) + 2\pi M^2 \sin 2\alpha_0 - K_2' \sin 2(\alpha_0 - \beta')$$
$$+ \frac{K_2'}{2} \sin 4(\alpha_0 - \beta') = 0 , \qquad (11)$$

and will change with temperature even if β and β' are independent of temperature due to the dependence of K_1 and K_2'.

Consider now the fixed-angle torque curves shown in Figs. 17(a) and 17(b). Introducing β and/or K_2 as in Eqs. (3) or (6) cannot produce an asymmetry between data taken at plus and minus angles relative to the easy axis, nor produce the extreme nonlinearity seen in Fig. 17(a). Introducing a second uniaxial anisotropy term such as $K_1' \sin^2(\theta - \beta')$, where $\beta' \neq \beta$, still does not produce an asymmetry, as $K_1 \sin^2(\theta - \beta) + K_1' \sin^2(\theta - \beta')$ can be combined into a single term $K_1'' \sin^2(\theta - \beta'')$; the torque curves would still be symmetric about an effective easy axis at an angle α_0'' related to β''. If, however, we assume that the anisotropy has the more complex form of Eq. (9), then both the 45° and low-angle plots are predicted to be asymmetric. Thus the form of the anisotropy given by Eq. (9) is the simplest that leads to an asymmetry. It also explains, as discussed above, the temperature dependence of α_0 shown in Fig. 13. It does not, however, explain the nonlinearities in H seen in the Fe-rich low-angle plots such as Fig. 17(a). Presumably a still more complicated form of the anisotropy is needed for that. We would like to mention here that the complicated, hypothetical, and

probably incomplete relationship between α_0 and β determined by Eq. (11) caused us to plot the measured angle α_0 in Figs. 10–15 rather than a calculated angle β. Furthermore, there is no reasonable single value which could be chosen as a measure of the magnitude of the anisotropy. Hence, none is plotted in Fig. 18.

It is likely that both β and β' are related to the incident angles of the atomic beams during the deposition. Thus we would expect that both would equal zero in samples rotated during growth, and, in fact, we observe that the effective easy axis $\alpha_0 = 0$. With both $\beta' = \beta = 0$, Eqs. (9) and (10) would reduce to the simpler form of Eq. (6). We would therefore not expect to see the anomalies in either the fixed-angle torque curves or in the temperature dependence of α_0 in Fe-rich rotated samples. (Practical details have precluded our taking these data to date.)

MODEL

We propose that the extra term in the anisotropy energy of the Fe-rich samples deposited at room temperature necessitated by the anomalies in the torque data are due to inclusions of a second phase with a strong local anisotropy. This second phase is embedded in an "amorphous" matrix in which the local arrangement is similar to that of the Tb-rich material. The strong dependence on deposition parameters of the direction of the easy axis, seen only in the Fe-rich material, also suggests a more complicated local arrangement than that in the Tb-rich material. While no structure is seen in TEM bright- or dark-field images, a slight difference in TEM diffraction patterns may be seen in Figs. 2 and 3. The Tb-rich samples show one faint ring outside the primary halo while Fe-rich samples grown at room temperature show two faint rings. We will assume that since the inclusions are invisible to the TEM images, they are small and hence the magnetic moment is exchange coupled to the amorphous matrix. There is therefore a single M, as has been implicitly assumed in all the equations above. Equation (9) describes the anisotropy associated with the inclusions, as well as the usual uniaxial anisotropy associated with the "amorphous" matrix.

The dependence of the direction of the easy axis on *deposition* temperature and other deposition parameters reflects two separate factors. The first is the ability of the a-Tb-Fe (both Tb and Fe rich) to form the nonrandom arrangement of atoms required to produce an anisotropy. Increasing deposition temperature will increasingly allow adatoms to find energetically favorable locations, thereby increasing the amount of ordering, whether of pairs, clusters, or inclusions of a second phase. This ordering occurs relative to the surface and will occur, for example, in samples rotated during deposition. The other factor necessary to observe the behavior presented in Figs. 10–17 is an incident angle. Because the incident angle of the atoms is not perpendicular, the growth direction is not quite perpendicular. In effect, the "surface" is not parallel to the substrate, but perpendicular to the growth direction. Thus the direction of the oriented pairs or clusters is not along the film normal, but rather along a direction related to the incident angles. This effect is fre-

quently seen in "diffusion-limited aggregation" with non-perpendicular incident atom beams.[20,21] During the growth of our samples, bombardment of the surface by energetic particles causes the atoms to have enough surface mobility to essentially eliminate the columnar microstructure associated with diffusion-limited aggregation and seen, for example, in a-Tb-Fe films prepared at the same deposition temperature but by diode rather than magnetron sputtering.[32] However, a residual effect of the incident angles empirically still remains. As the deposition temperature increases, surface mobility will reduce the effect of the incident angles. Thus the two factors have competing temperature dependencies. Figure 15, which shows the angle of the easy axis for samples grown at 77 K, shows a large tilt, due to the strong input of the incident angles, but no discontinuity, because the second phase did not form. Some type of ordering, pairs or clusters, is still present and causes a perpendicular anisotropy, but of reduced magnitude. We are primarily interested in the first factor, the local ordering, but depend on the second factor to examine it.

For both Tb- and Fe-rich a-Tb-Fe, the angle β and β' would be expected to be a function of the incident angles of the atoms. Apparently, based on Fig. 11, the orientation of the second-phase inclusions on the Fe-rich side is far more sensitive than the orientation of the local structure in the "amorphous" phase found on the Tb-rich side. The crossover from negative angles to positive angles near 15 at. % Tb seen in Fig. 11 occurs for each set of data at almost exactly the position in the row of samples at which the average incident angle crosses over from negative to positive.[45] Examining Fig. 11 more closely, one fact is unexplained by the idea of inclusions whose angle is determined by the incident angles of the atoms. Holding composition fixed, consider the angle of the easy axis α_0 for the three sets of incident angles represented. Between 17 and 20 at. % Tb, α_0 *decreases* with increasing average angle. A more detailed understanding of the formation of the second phase is necessary to explain this peculiar fact.

The formation of the inclusions is affected by film thickness, as seen in Fig. 12. It is possible that they are unable to nucleate in the thin films.

We would like to propose two possible models for the transition at 22 at. % Tb and two corresponding etiologies of the second phase introduced above in the description of the Fe-rich material. The first possibility is that there are two different amorphous phases characterized by different local arrangements. The composition dependence of the free energy of the two phases is different. A metastable phase diagram of the amorphous phase may be drawn by considering the minimum free energy without allowing crystallization. (The high crystallization temperature of a-Tb-Fe is presumably due to a high energy barrier to nucleation of crystallites.) Above 22 at. % Tb, amorphous phase 1 is the metastable phase. It is insensitive to deposition parameters and could perhaps consist primarily of the icosahedral clusters suggested by several scientists to form the basis of the amorphous state.[14,46−49] Icosahedral clusters are not expected to produce high magnetic anisotropy due to a high symme-

try;[50] however, this analysis was performed for monatomic materials. Chemical ordering of the two elements, Tb and Fe, in each icosahedral cluster relative to the film surface could presumably produce a high uniaxial anisotropy. Below 22 at. % Tb, the material is in a two-phase region consisting of amorphous phase 1 plus increasing amounts of amorphous phase 2. This second phase is sensitive to deposition parameters and could perhaps consist primarily of the octahedral clusters typical of the bcc phase of α-Fe, the local clusters found in the nearby intermetallic compound Tb_6Fe_{23} (Ref. 51) or possibly larger clusters. These clusters would of course be the inclusions discussed above. The Fe-rich border of the two-phase field cannot be estimated from the data. Two distinct amorphous phases have been previously suggested for various TM-TM and TM-metalloid glasses.[52−57]

The other possibility is that, while we are far from actually crystallizing the samples, as may be seen from Fig. 4, there could be precursor precipitates of diameter less than 20 Å. The a-RE-TM alloys have occasionally been claimed to precipitate out the pure elemental phases, in this case α-Fe and α-Tb, long before crystallization occurs.[58,59] While this is not theoretically energetically impossible, it is unexpected when several intermetallic compounds exist at nearby compositions. If the common tangent between α-Fe and the amorphous phase was at 22 at. % Tb, Fe-rich samples could precipitate α-Fe, leaving behind Tb-richer a-Tb-Fe. It would, however, be *energetically impossible* for Tb-rich samples to precipitate α-Fe unless a low free-energy Tb-rich crystalline phase was simultaneously precipitated, a process requiring more nucleation energy. α-Tb alone could perhaps precipitate, but it is farther away than α-Fe in composition space and, hence, less could precipitate. Furthermore, the low Curie temperature of α-Tb would suggest that it should have a weaker effect on magnetic properties.

In both cases, diffusion and precipitation of a second phase is required. These processes are evidently kinetically prevented in samples grown at 77 K by the low surface mobility of the adatoms, explaining the simple uniaxial anisotropy of these samples.

In either model there should not be an abrupt transition in the properties. The amount of amorphous phase 2 or the amount of α-Fe should be directly proportional to the difference between the composition of the sample and 22 at. % Tb. These amounts should thus go to zero continuously. A gradual transition in the properties must be hidden by the composition region near 22 at. % Tb, which we cannot measure due to the low magnetic moment.

It is also possible that precursor precipitates are related to the presence of the equilibrium intermetallic compound Tb_6Fe_{23} at 20.7 at. % Tb.[60] Precipitates of less than 20 Å would be approximately one unit cell of its relatively complex structure.[51] It is possible that this compound might precipitate out when no diffusion is required, i.e., for compositions near 20.7 at. % Tb. It is not, however, obvious why precipitates should form beginning at ≈ 21 at. % Tb and continuing down to at least 15 at. % Tb. Their volume fraction would presumably maximize at 20.7 at. % Tb and decrease as the composi-

tion decreases, somewhat consistently with the observed data. A detailed thermodynamically correct model of this process is not obvious. It is also not obvious why the other intermetallic compounds with simpler structures (such as $TbFe_2$ or $TbFe_3$,[60] which are magnetic) do not form at compositions near to theirs. Furthermore, the precipitate explanation is somewhat unsatisfying in general in that it is not obvious why tiny "precursor" precipitates could form in samples deposited at room temperature and yet fail to manifest themselves in x-ray diffraction on samples deposited as high as 400 or even 600 °C, as discussed previously and shown in Fig. 4.

CONCLUSIONS

Amorphous Tb-Fe samples prepared under a variety of deposition conditions have been extensively characterized by both magnetic and structural measurements. The direction of the easy axis and the dependence of the torque on applied magnetic field at various fixed angles have revealed a transition with changing composition within what is typically called the amorphous state, as judged by TEM and x-ray diffraction. The magnetic anisotropy energy of Tb-rich a-Tb-Fe (containing more than 22 at. % Tb) can be written in a simple uniaxial form: $K_1\sin^2(\theta-\beta)+K_2\sin^4(\theta-\beta)$, where β reflects the effect of the incident angles of the Tb and Fe atoms during growth of the films. The source of this anisotropy appears, at least in these films, to be predominantly microscopic, and we would favor the model that the local clusters, which would be found in amorphous Tb-Fe prepared by any technique, are oriented by the film-growth process.

The magnetic anisotropy energy of the Fe-rich material grown at room temperature, by contrast, requires a more complex form containing higher-order terms at two *different* angles: $K_1\sin^2(\theta-\beta)+K_2\sin^4(\theta-\beta)+K_1'\sin^2(\theta-\beta')+K_2'\sin^4(\theta-\beta')$, where both β and β' are presumably related to the incident angles of the

atoms during deposition. This form explains much of the data of Fe-rich a-Tb-Fe, but still fails to explain the nonlinearities seen in Fig. 17(a). The transition occurs relatively abruptly at 22 at. % Tb, the room-temperature magnetic compensation composition. However, results on samples grown above the Curie temperature suggest that this coincidence is accidental. The region between 21 and 23 at. % Tb is immeasurable due to the low moment.

This dramatic transition in the form of the magnetic anisotropy energy must reflect a change in the local structure. The transition is not seen in the gross magnetic properties such as $M(T)$ or T_C. The extra term in the anisotropy energy of the Fe-rich material is suggested to originate in second-phase inclusions which are embedded in an amorphous matrix. *Detection* of this second phase by magnetic measurements appears to require nonperpendicular deposition angles. The source of the second phase is suggested to be either the presence of two distinct amorphous phases with different local structures or precursor precipitates of α-Fe or possibly Tb_6Fe_{23}. The precipitates must be less than 20 Å as they are invisible to TEM. The second amorphous phase would probably not appear distinct to the TEM and so could be larger than 20 Å. These second-phase inclusions do not occur in Fe-rich samples grown at 77 K; their magnetic anisotropy is simply uniaxial. It is likely that the reduced surface mobility during growth at 77 K kinetically limits the formation of the second phase. Further investigation by Mössbauer or extended x-ray-absorption fine-structure measurements could yield valuable information and provide direct structural evidence of the change in local order.

ACKNOWLEDGMENTS

*Present address: Department of Physics, University of California, San Diego, La Jolla, CA 92093.

[1]Tu Chen, D. Cheng, and G. B. Charlan, IEEE Trans. Magn. MAG-16, 1194 (1980).

[2]Y. Togami, IEEE Trans. Magn. MAG-18, 1233 (1982).

[3]M. H. Kryder, J. Appl. Phys. 57, 3913 (1985).

[4]Y. Mimura and N. Imamura, Appl. Phys. Lett. 28, 746 (1976).

[5]N. Heiman, A. Onton, D. F. Kyser, K. Lee, and C. R. Guarnieri, in *Magnetism Magnetic Materials (San Francisco, 1974)*, Proceedings of the 20th Annual Conference on Magnetism and Magnetic Materials, AIP Conf. Proc. No. 24, edited by C. D. Graham, Jr., G. H. Lander, and J. J. Rhyne (AIP, New York, 1975), p. 573.

[6]S. S. Nandra and P. J. Grundy, Phys. Status Solidi A 41, 65 (1977).

[7]H. Kobayashi, T. Ono, A. Tsushima, and T. Suzuki, Appl. Phys. Lett. 43, 389 (1983).

[8]R. B. van Dover, M. Hong, E. M. Gyorgy, J. F. Dillon, Jr., and

S. D. Albiston, J. Appl. Phys. 57, 3897 (1985).

[9]R. J. Gambino, P. Chaudhari, and J. J. Cuomo, in *Magnetism and Magnetic Materials (Denver, 1972)*, Proceedings of the 18th Annual Conference on Magnetism and Magnetic Materials, AIP Conf. Proc. No. 18, edited by C. D. Graham, Jr. and J. J. Rhyne (AIP, New York, 1973), p. 578.

[10]R. J. Gambino, J. Ziegler, and J. J. Cuomo, Appl. Phys. Lett. 24, 99 (1974).

[11]Y. Nishihara, T. Katayama, Y. Yamaguchi, S. Ogawa, and T. Tsushima, Jpn. J. Appl. Phys. 17, 1083 (1978).

[12]T. Egami, in *Amorphous Metallic Alloys*, edited by F. E. Luborsky (Butterworths, London, 1983), p. 100.

[13]M. R. Hoare, Ann. N. Y. Acad. Sci. 279, 186 (1976).

[14]C. L. Briant and J. J. Burton, Phys. Status Solidi B 85, 393 (1978).

[15]P. Chaudhari and D. Turnbull, Science 199, 11 (1978).

[16]T. Egami, C. D. Graham, Jr., W. Dmowski, P. Zhou, P. J. Flanders, E. E. Marinero, H. Notarys, and C. Robinson,

IEEE Trans. Magn. MAG-23, 2269 (1987).

[17]R. Zwingman, W. L. Wilson, Jr., and H. C. Bourne, Jr., in *Magnetism and Magnetic Materials, 1976 (Joint MMM–Intermag Conference, Pittsburgh)*, Partial Proceedings of the First Joint MMM–Intermag Conference, AIP Conf. Proc. No. 34, edited by J. J. Becker and G. H. Lander (AIP, New York, 1976), p. 334.

[18]D. W. Forester, C. Vittoria, J. Schelleng, and P. Lubitz, J. Appl. Phys. 49, 1966 (1978).

[19]H. Takagi, S. Tsunashima, S. Uchiyama, and T. Fujii, J. Appl. Phys. 50, 1642 (1979).

[20]N. G. Nakhodkin and A. I. Shaldervan, Thin Solid Films 10, 109 (1972).

[21]A. G. Dirks and H. J. Leamy, Thin Solid Films 47, 219 (1977).

[22]S. Esho and S. Fujiwara, in Ref. 17, p. 331.

[23]J. F. Graczyk, in Ref. 17, p. 343.

[24]H. Hoffman and R. Winkler, J. Magn. Magn. 13, 89 (1979).

[25]Y. Yafet, E. M. Gyorgy, and L. R. Walker, J. Appl. Phys. 60, 4236 (1986).

[26]T. Mizoguchi and G. S. Cargill, III, J. Appl. Phys. 50, 3570 (1979).

[27]C. N. J. Wagner, N. Heiman, T. C. Huang, A. Onton, and W. Parrish, in *Magnetism and Magnetic Materials (Philadelphia, 1975)*, Proceedings of the 21st Annual Conference on Magnetism and Magnetic Materials, AIP Conf. Proc. No. 29, edited by J. J. Becker, G. H. Lander, and J. J. Rhyne (AIP, New York, 1976), p. 188.

[28]L. J. Maksymowicz, L. Dargel, M. Lubecka, and M. Pyka, J. Magn. Magn. 35, 281 (1983).

[29]C. G. Windsor, D. S. Boudreaux, and M. C. Narasimhan, Phys. Lett. 67A, 282 (1978).

[30]K. Suzuki, in *Proceedings of the 4th International Conference on Rapidly Quenched Metals*, edited by T. Masumoto and K. Suzuki (Japan Institute of Metals, Sendai, 1982), Vol. 1, p. 309.

[31]Y. Suzuki, J. Haimovich, and T. Egami, Phys. Rev. B 35, 2162 (1987).

[32]S. Nakahara, M. Hong, R. B. van Dover, E. M. Gyorgy, and D. D. Bacon, J. Vac. Sci. Technol. A 4, 543 (1986).

[33]Y. Takeno, M. Suwabe, and K. Goto, IEEE Trans. Magn. MAG-23, 2141 (1987).

[34]F. Hellman, R. B. van Dover, and E. M. Gyorgy, Appl. Phys. Lett. 50, 296 (1987).

[35]H. S. Chen (private communication).

[36]Y. Mimura, N. Imamura, T. Kobayashi, A. Okada, and Y. Kushiro, J. Appl. Phys. 49, 1208 (1978).

[37]J. F. Dillon, Jr., R. B. van Dover, M. Hong, E. M. Gyorgy, and S. D. Albiston, J. Appl. Phys. 61, 1103 (1987).

[38]S. Chikazumi, *Physics of Magnetism* (Wiley, New York, 1964), p. 130.

[39]H. B. Collen and E. Callen, J. Phys. Chem. Solids 27, 1271 (1966).

[40]Hideki Miyajima, Katsuo Sato, and Tadashi Mizoguchi, J. Appl. Phys. 47, 4669 (1976).

[41]S. Chikazumi, J. Appl. Phys. 32, 81S (1961).

[42]P. Wolniansky, S. Chase, R. Rosenvold, M. Ruane, and M. Mansuripur, J. Appl. Phys. 60, 346 (1986).

[43]M. Hong, E. M. Gyorgy, and D. D. Bacon, Appl. Phys. Lett. 44, 706 (1984).

[44]J. J. Rhyne, S. J. Pickart, and H. A. Alperin, Phys. Rev. Lett. 29, 1562 (1972); J. J. Rhyne, J. H. Schelleng, and N. C. Koon, Phys. Rev. B 10, 4672 (1974).

[45]The average incident angle is defined to be the sum of the Tb and Fe atoms' incident angles weighted by the atomic percentage of each element for the composition.

[46]F. C. Frank, Proc. R. Soc. London, Ser. A 215, 43 (1952).

[47]R. C. O'Handley, M. E. McHenry, H. Li, D. Kofalt, and T. Egami, IEEE Trans. Magn. MAG-22, 421 (1986).

[48]P. J. Steinhardt, D. R. Nelson, and M. Ronchetti, Phys. Rev. B 28, 784 (1983).

[49]D. R. Nelson, Phys. Rev. B 28, 5515 (1983).

[50]M. E. McHenry, R. C. O'Handley, W. Dmowski, and T. Egami, J. Appl. Phys. 61, 4232 (1987).

[51]J. V. Florio, R. E. Rundle, and A. I. Snow, Acta Crystallogr. 5, 449 (1952).

[52]S. T. Hopkins and W. L. Johnson, Solid State Commun. 43, 537 (1982).

[53]D. S. Lashmore, L. H. Bennett, H. E. Schone, P. Gustafson, and R. E. Watson, Phys. Rev. Lett. 48, 1760 (1982).

[54]B. W. Corb, R. C. O'Handley, J. Megusar, and N. J. Grant, Phys. Rev. Lett. 51, 1386 (1983).

[55]H. U. Krebs, D. J. Webb, and A. F. Marshall, Phys. Rev. B 35, 5392 (1987).

[56]C. Michaelson, H. A. Wagner, and H. C. Freyhardt, J. Phys. F 16, 109 (1986).

[57]G. Suran, K. Ounadjela, and F. Machizaud, Phys. Rev. Lett. 57, 3109 (1986).

[58]K. H. J. Buschow and A. G. Dirks, J. Electrochem. Soc. 127, 2430 (1980).

[59]S. R. Lee and A. E. Miller, J. Appl. Phys. 55, 3465 (1984).

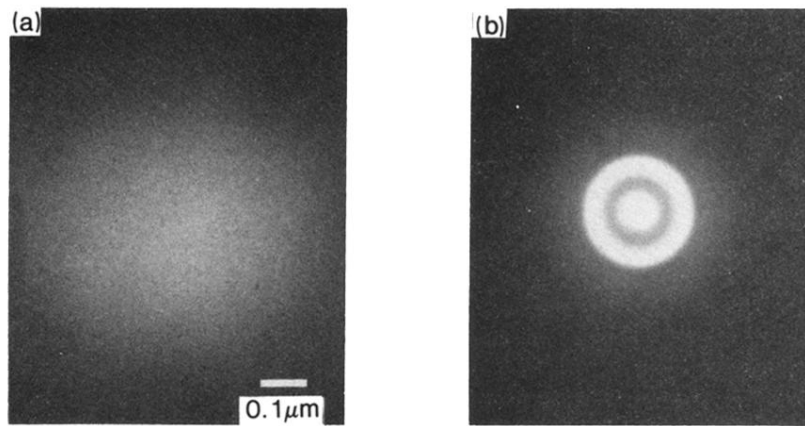[60]M. P. Dariel, J. T. Holthuis, and M. R. Pickus, J. Less-Common Met. 45, 91 (1976).

FIG. 2. TEM bright-field and selected-area diffraction images of a-Tb-Fe containing 24 at. % Tb.
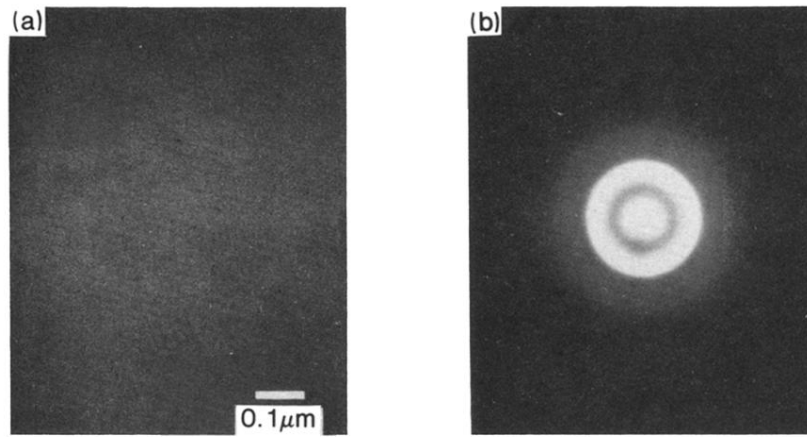
FIG. 3. TEM bright-field and selected-area diffraction images of a-Tb-Fe containing 17 at. % Tb.